Shock Wave Structure in Polyatomic Gases: Numerical Analysis Using a Model Boltzmann Equation

Shingo Kosuge
Kazuo Aoki
Takashi Goto

NCTS/Math Technical Report
2016-008

National Center for
Theoretical Sciences
Mathematics Division, Taiwan

Shock Wave Structure in Polyatomic Gases: Numerical Analysis Using a Model Boltzmann Equation

Shingo Kosuge[1,a)], Kazuo Aoki[2] and Takashi Goto[3]

[1]*Center for Global Leadership Engineering Education, Graduate School of Engineering, Kyoto University, Kyoto 615-8540, Japan*
[2]*National Center for Theoretical Sciences, National Taiwan University, Taipei 10617, Taiwan and Department of Mathematics, National Cheng Kung University, Tainan 70101, Taiwan*
[3]*Department of Mechanical Engineering and Science, Graduate School of Engineering, Kyoto University, Kyoto 615-8540, Japan*

[a)]Corresponding author: kosuge.shingo.6r@kyoto-u.ac.jp

Abstract. The structure of a standing plane shock wave in a polyatomic gas is investigated on the basis of kinetic theory, with special interest in the CO_2 gas. The polyatomic version of the ellipsoidal statistical model is employed, and the shock structure is obtained numerically for several Mach numbers for a pseudo-CO_2 gas, which is an artificial CO_2 gas with smaller ratio of the bulk viscosity to the viscosity. The double-layer structure consisting of a thin upstream layer with a steep change and a much thicker downstream layer with a mild change, which has been known for a long time and was confirmed recently by the extended thermodynamics [S. Taniguchi *et al.*, Int. J. Non-Linear Mech. **79**, 66 (2016)], is reproduced.

INTRODUCTION

The structure of a standing plane shock wave is one of the most fundamental problems in kinetic theory of gases and has been investigated by many researchers experimentally, theoretically, and numerically since 1960's (cf. [1, 2, 3, 4, 5, 6]). In the present study, we focus our attention on a polyatomic gas, in particular, carbon dioxide (CO_2) gas. Recently, the shock-structure problem for a polyatomic gas was investigated numerically by using extended thermodynamics [7, 8, 9], and some interesting results were reported. In the first paper [7], the case of relatively weak shock was considered, and it was shown that for a CO_2 gas, the profiles of macroscopic quantities exhibit three different types (Types A, B, and C in [7, 8, 9]) depending on the Mach number. When the Mach number is close to 1, the profiles are almost symmetric with respect to the center of the profile of each macroscopic variable (Type A). As the Mach number increases slightly, the profiles become nonsymmetric (Type B). A further (slight) increase of the Mach number leads to profiles with a double-layer structure, consisting of a thin layer with steep change and a thick layer over which the quantities slowly approach the downstream equilibrium values. The Type C profiles have been confirmed for higher Mach numbers ($M = 1.3$, 3, and 5, where M is the Mach number) numerically on the basis of the nonlinear extended thermodynamics [9]. The existence of the Type-C profiles had been known for a long time (see *Introduction* in [7, 9] and references therein). However, the recent results in [7, 8, 9] are, according to the authors of these references, the first results based on a unified theory using a single equation for both the thin and thick layers.

Although some theoretical and numerical discussions to validate the nonlinear extended thermodynamics for polyatomic rarefied gases in a strong nonequilibrium case are made in [9], its validity should also be confirmed by kinetic theory. However, as mentioned in *Introduction* in [7, 9], it is not an easy task because of the complexity of the collision integral of the Boltzmann equation for a polyatomic gas. In order to apply kinetic theory, therefore, one cannot avoid introducing some phenomenological models at some point in the theory or numerics. Nevertheless, it is still interesting to see whether the Type-C solution can be found for a CO_2 gas on the basis of kinetic theory. This is the motivation of the present study.

This note contains some preliminary computations based on kinetic theory. More specifically, we adopt the polyatomic version of the ellipsoidal statistical (ES) model [10], which was proposed in [11] and was rederived in

a systematic way in [12]. This equation has a simple structure that the internal degrees of freedom are expressed by an additional (continuous) energy variable associated with the internal modes. Although it is simple, it satisfies basic properties of the Boltzmann equation for a polyatomic gas [11], such as the conservation laws and the H-theorem [13]. It is known that the ratio of the bulk viscosity to the viscosity of CO_2 gas is quite large and is of the order of 1000. This large value of the ratio causes a large shock thickness, which gives a computational difficulty, since a very large computational domain is required. For this reason, we consider in this study an artificial CO_2 gas with a smaller values of the ratio (≤ 100), which will be called a pseudo-CO_2 gas. Such a gas, which gives a shorter shock thickness and hopefully retains the qualitative properties of the CO_2 gas, facilitates the computation.

As will be seen, the pseudo-CO_2 gases with increasing ratio of the bulk viscosity to the viscosity tend to reproduce the double-layer structure (Type-C) well. From this tendency, we will estimate the shock thickness of the CO_2 gas.

PROBLEM AND ASSUMPTIONS

We consider a stationary plane shock wave standing in a flow of an ideal polyatomic gas. We take the X_1 axis of the coordinate system (X_1, X_2, X_3) normal to the shock wave. The gas at upstream infinity ($X_1 \to -\infty$) is in an equilibrium state with density ρ_-, flow velocity $\boldsymbol{u}_- = (u_-, 0, 0)$, and temperature T_-, whereas that at downstream infinity ($X_1 \to \infty$) is in another equilibrium state with density ρ_+, flow velocity $\boldsymbol{u}_+ = (u_+, 0, 0)$, and temperature T_+. We investigate the steady behavior of the gas under the following assumptions: (i) The behavior of the gas is described by the ellipsoidal statistical (ES) model of the Boltzmann equation for a polyatomic gas [11, 12]; (ii) The problem is spatially one-dimensional, so that the physical quantities are independent of X_2 and X_3.

Let γ be the ratio of the specific heats, $\gamma = c_p/c_v$, where c_p and c_v are the specific heat at constant pressure and that at constant volume, respectively. Then, it is expressed in terms of the internal degrees of freedom δ of a molecule as

$$\gamma = (\delta + 5)/(\delta + 3). \tag{1}$$

If we denote by M the upstream Mach number of the flow, $M = u_-/\sqrt{\gamma R T_-}$, where R is the specific gas constant ($R = k/m$ with the Boltzmann constant k and the mass of a molecule m), the downstream quantities ρ_+, u_+, and T_+ are expressed in terms of the upstream quantities ρ_-, u_-, and T_- and M by the Rankine–Hugoniot relations:

$$\rho_+ = \frac{(\gamma+1)M^2}{(\gamma-1)M^2+2}\,\rho_-, \tag{2a}$$

$$u_+ = \frac{(\gamma-1)M^2+2}{(\gamma+1)M^2}\,u_-, \tag{2b}$$

$$T_+ = \frac{[2\gamma M^2-(\gamma-1)][(\gamma-1)M^2+2]}{(\gamma+1)^2M^2}\,T_-. \tag{2c}$$

BASIC EQUATIONS

Let $\boldsymbol{X}$ (or X_i) be the position vector in space, $\boldsymbol{\xi}$ (or ξ_i) the molecular velocity vector, and $\mathcal{E}$ the energy associated with the internal degrees of freedom and let $d\boldsymbol{X} = dX_1dX_2dX_3$ and $d\boldsymbol{\xi} = d\xi_1d\xi_2d\xi_3$. We denote the number of molecules contained in an infinitesimal volume $d\boldsymbol{X}d\boldsymbol{\xi}d\mathcal{E}$ around a point ($\boldsymbol{X}$, $\boldsymbol{\xi}$, $\mathcal{E}$) in the seven-dimensional space $\boldsymbol{X}$-$\boldsymbol{\xi}$-$\mathcal{E}$ as

$$(1/m)\, f(t, \boldsymbol{X}, \boldsymbol{\xi}, \mathcal{E}) d\boldsymbol{X}d\boldsymbol{\xi}d\mathcal{E}, \tag{3}$$

where f is the velocity and internal energy distribution function.

The ES model in the present steady and spatially one-dimensional problem, where $f = f(X_1, \boldsymbol{\xi}, \mathcal{E})$, reads

$$\xi_1 \frac{\partial f}{\partial X_1} = A_{\mathrm{c}}(T)\rho(\mathcal{G} - f), \tag{4}$$

where

$$\mathcal{G} = \frac{\rho\Lambda_\delta \mathcal{E}^{\delta/2-1}}{(2\pi)^{3/2}\sqrt{\det(\underline{\mathcal{T}})}(RT_{\mathrm{rel}})^{\delta/2}} \exp\left(-\frac{1}{2}(\xi_i - u_i)(\underline{\mathcal{T}}^{-1})_{ij}(\xi_j - u_j) - \frac{\mathcal{E}}{RT_{\mathrm{rel}}}\right), \tag{5a}$$

$$(\underline{\mathcal{T}})_{ij} = (1-\eta)[(1-\nu)RT_{\rm tr}\delta_{ij} + \nu p_{ij}/\rho] + \eta RT\delta_{ij}, \tag{5b}$$

$$\rho = \iint_0^\infty f d\mathcal{E} d\boldsymbol{\xi}, \qquad u_i = \frac{1}{\rho}\iint_0^\infty \xi_i f d\mathcal{E} d\boldsymbol{\xi}, \qquad p_{ij} = \iint_0^\infty (\xi_i - u_i)(\xi_j - u_j) f d\mathcal{E} d\boldsymbol{\xi}, \tag{5c}$$

$$T_{\rm tr} = \frac{1}{3R\rho}\iint_0^\infty (\xi_k - u_k)^2 f d\mathcal{E} d\boldsymbol{\xi}, \qquad T_{\rm int} = \frac{2}{\delta R\rho}\iint_0^\infty \mathcal{E} f d\mathcal{E} d\boldsymbol{\xi}, \tag{5d}$$

$$T = \frac{3T_{\rm tr} + \delta T_{\rm int}}{3+\delta}, \qquad T_{\rm rel} = \eta T + (1-\eta)T_{\rm int}. \tag{5e}$$

Here, ρ is the density, $u_i = (u,\, 0,\, 0)$ the flow velocity, p_{ij} the stress tensor, $T_{\rm tr}$ the temperature associated with translational motion, $T_{\rm int}$ the temperature associated with the energy of the internal degree of freedom, T the temperature, and the domain of integration with respect to $\boldsymbol{\xi}$ is the whole space of $\boldsymbol{\xi}$. The symbol δ_{ij} indicates the Kronecker delta, and $\nu \in [-1/2,\, 1)$ and $\eta \in (0,\, 1]$ are the constants that adjust the Prandtl number and the bulk viscosity. The $A_{\rm c}(T)$ is a function of T such that $A_{\rm c}(T)\rho$ is the collision frequency of the gas molecules. The Λ_δ in Eq. (5a) is a dimensionless constant defined by

$$\Lambda_\delta = \left(\int_0^\infty s^{\delta/2-1}{\rm e}^{-s} ds\right)^{-1}. \tag{6}$$

The $\underline{\mathcal{T}}$ is the 3×3 matrix the $(i,\, j)$ component of which is given by Eq. (5b), and $\det(\underline{\mathcal{T}})$ and $\underline{\mathcal{T}}^{-1}$ are, respectively, its determinant and inverse.

For Eq. (4), the viscosity μ, the thermal conductivity κ, the Prandtl number Pr, and the bulk viscosity μ_b are derived in the following form:

$$\mu = \frac{1}{1-\nu+\eta\nu}\frac{RT}{A_{\rm c}(T)}, \qquad \kappa = \frac{\gamma}{\gamma-1}R\frac{RT}{A_{\rm c}(T)}, \qquad {\rm Pr} = \frac{1}{1-\nu+\eta\nu}, \qquad \mu_b = \frac{1}{\eta}\left(\frac{5}{3}-\gamma\right)\frac{\mu}{\rm Pr}. \tag{7}$$

The boundary condition at upstream infinity and that at downstream infinity are as follows:

$$f = \frac{\rho_-\Lambda_\delta}{(2\pi RT_-)^{3/2}(RT_-)^{\delta/2}}\mathcal{E}^{\delta/2-1}\exp\left(-\frac{(\xi_1-u_-)^2+\xi_2^2+\xi_3^2}{2RT_-} - \frac{\mathcal{E}}{RT_-}\right), \qquad (X_1 \to -\infty), \tag{8a}$$

$$f = \frac{\rho_+\Lambda_\delta}{(2\pi RT_+)^{3/2}(RT_+)^{\delta/2}}\mathcal{E}^{\delta/2-1}\exp\left(-\frac{(\xi_1-u_+)^2+\xi_2^2+\xi_3^2}{2RT_+} - \frac{\mathcal{E}}{RT_+}\right), \qquad (X_1 \to \infty). \tag{8b}$$

NUMERICAL ANALYSIS

One of the advantages of using Eq. (4) is that one can reduce the independent variables from $(X_1,\, \xi_1,\, \xi_2,\, \xi_3,\, \mathcal{E})$ to $(X_1,\, \xi_1)$ eliminating the molecular velocity components ξ_2 and ξ_3 parallel to the shock and the energy variable $\mathcal{E}$ in the present spatially one-dimensional problem. More specifically, we introduce the following three marginal velocity distribution functions:

$$g(X_1,\, \xi_1) = \iint_{-\infty}^\infty \int_0^\infty f(X_1,\, \xi_1,\, \xi_2,\, \xi_3,\, \mathcal{E}) d\mathcal{E} d\xi_2 d\xi_3, \tag{9a}$$

$$h(X_1,\, \xi_1) = \iint_{-\infty}^\infty \int_0^\infty (\xi_2^2+\xi_3^2) f(X_1,\, \xi_1,\, \xi_2,\, \xi_3,\, \mathcal{E}) d\mathcal{E} d\xi_2 d\xi_3, \tag{9b}$$

$$i(X_1,\, \xi_1) = \iint_{-\infty}^\infty \int_0^\infty \mathcal{E} f(X_1,\, \xi_1,\, \xi_2,\, \xi_3,\, \mathcal{E}) d\mathcal{E} d\xi_2 d\xi_3. \tag{9c}$$

If we multiply Eq. (4) by 1, $\xi_2^2+\xi_3^2$, and $\mathcal{E}$ and integrate the respective results over $-\infty < \xi_2,\, \xi_3 < \infty$ and $0 < \mathcal{E} < \infty$, then we obtain three simultaneous integro-differential equations of ES type for g, h, and i. It should be noted that the resulting equations do not contain the energy variable $\mathcal{E}$ associated with the internal degrees of freedom. The boundary conditions for these equations at $X_1 \to \pm\infty$ can be obtained by a similar procedure. Here, we omit the resulting equations and boundary conditions because of limited space. It should be noted that, though the elimination of ξ_2 and ξ_3 is possible only for spatially one-dimensional problems [14], that of $\mathcal{E}$ is always possible [11].

The equations for g, h, and i are solved numerically by a finite-different method similar to that used in [15]. More precisely, we add the time-derivative terms $\partial g/\partial t$, $\partial h/\partial t$, and $\partial i/\partial t$ to the respective equations and pursue the time evolution of the solution for a long time. We regard the numerically obtained long-time limit as the steady solution. Since we do not give the details of the numerical scheme, we also omit the data for the computational system. We only mention that we use uniform grids for X_1, the size of which is sufficiently smaller than the mean free path.

NUMERICAL RESULTS

In the present paper, we mainly focus our attention on the structure of the shock wave in the CO_2 gas. But, in order to contrast its peculiar nature, we also present some results for the N_2 gas. In the present paper, we set $A_c(T)$ in Eq. (4) as $A_c(T) = CT$ with a constant C. This choice is unphysical because the viscosity, thermal conductivity, and bulk viscosity all become constant independent of the temperature. However, in the present preliminary step, this choice does not seem to have an essential effect on the qualitative features that will be discussed in the following subsections.

Shock structure in N_2 gas

We first show the structure of a shock wave in the N_2 gas. We set $\delta = 2$, i.e., $\gamma = 7/5$ [cf. Eq. (1)]. For N_2 gas at 293K, $\mu_b/\mu = 0.73$ ([16]) and Pr $= 0.723$ ([17]). These values give $\nu = -0.774$ and $\eta = 0.505$ [cf. Eq. (7)], and this ν is outside the admissible range ($\nu \in [-1/2, 1)$). Therefore, we set $\nu = -0.5$ and $\eta = 0.46$ here, which lead to $\mu_b/\mu = 0.736$ and Pr $= 0.787$. The Prandtl number is slightly larger, but we do not expect large effect from this difference.

Figure 1 shows the profiles of the density, flow velocity (the X_1 component), and temperature across the shock wave for $M = 1.2$ [Fig. 1(a)], 2.0 [Fig. 1(b)], and 5.0 [Fig. 1(c)]. To be more specific, we plot the quantities $\hat{\rho}$, $\hat{u}$, and $\hat{T}$ normalized in a conventional way, i.e.,

$$\hat{\rho} = \frac{\rho - \rho_-}{\rho_+ - \rho_-}, \qquad \hat{u} = \frac{u - u_+}{u_- - u_+}, \qquad \hat{T} = \frac{T - T_-}{T_+ - T_-}, \tag{10}$$

versus X_1/l_-, where l_- is the mean free path of the gas molecules at the equilibrium state at rest with density ρ_- and temperature T_-, i.e., $l_- = (2/\sqrt{\pi})(2RT_-)^{1/2}/A_c\rho_-$. In the figure, the solid line indicates $\hat{\rho}$, the dashed line $\hat{u}$, and the dot-dashed line $\hat{T}$, and the origin $X_1 = 0$ is set at the point where $\rho = (\rho_- + \rho_+)/2$, that is, $\hat{\rho} = 1/2$.

As the Mach number increases, the shock naturally becomes thinner, and thus the profile becomes steep. However, the qualitative features of the shock profiles do not differ much from the case of a monatomic gas.

Shock structure in pseudo-CO_2 gas

Next, we consider the CO_2 gas. Here, we set $\delta = 3$, i.e., $\gamma = 4/3$ [cf. Eq. (1)] and Pr $= 0.767$ [17]. According to [16], the value of μ_b/μ is quite large and is of the order of 1000. As we will explain later, the large values of μ_b/μ give rise

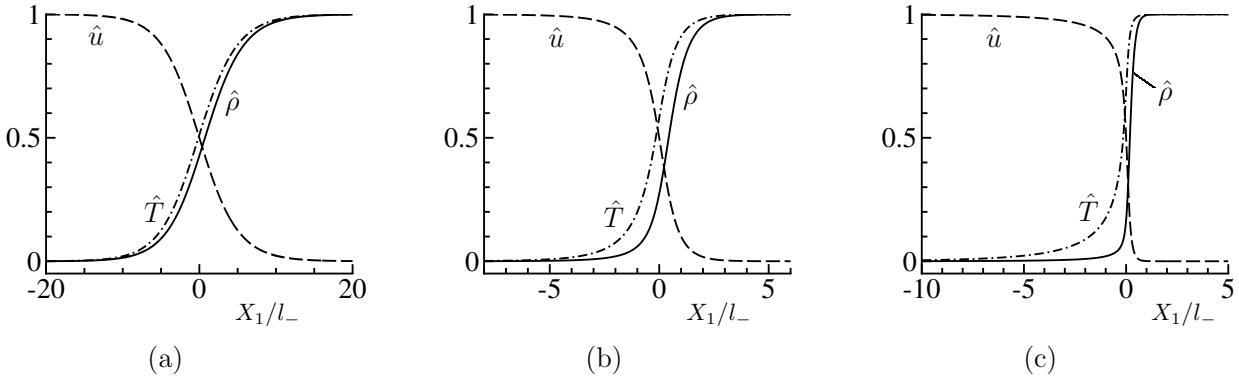

FIGURE 1. Profiles of the normalized density $\hat{\rho}$, flow velocity $\hat{u}$, and temperature $\hat{T}$ for N_2. (a) $M = 1.2$, (b) $M = 2.0$, and (c) $M = 5.0$.

TABLE 1. Values of ν and η for the pseudo-CO_2 gases with $\delta = 3$ and Pr = 0.767.

	μ_b/μ	ν	η
CO_2-(5)	5	−0.332	8.69×10^{-2}
CO_2-(10)	10	−0.318	4.35×10^{-2}
CO_2-(20)	20	−0.311	2.17×10^{-2}
CO_2-(30)	30	−0.308	1.45×10^{-2}
CO_2-(40)	40	−0.307	1.09×10^{-2}
CO_2-(50)	50	−0.306	8.69×10^{-3}
CO_2-(100)	100	−0.305	4.35×10^{-3}
CO_2-(1000)	1000	−0.303	4.34×10^{-4}

to computational difficulties. Therefore, we use smaller artificial values μ_b/μ = 5, 10, 20, 30, 40, 50, and 100 and try to infer the shock thickness when $\mu_b/\mu = 1000$. We call this gas with the artificial values of μ_b/μ the pseudo-CO_2 gases and denote them as CO_2-(value of μ_b/μ), for instance, CO_2-(100) means the gas with $\gamma = 4/3$, Pr = 0.767, and $\mu_b/\mu = 100$. The corresponding values of ν and η are listed in Table 1.

Figure 2 shows the profiles of $\hat{\rho}$, $\hat{u}$, and $\hat{T}$ [cf. Eq. (10)] at $M = 1.2$ [Fig. 2(a)], 2.0 [Fig. 2(b)], and 5.0 [Fig. 2(c)] for CO_2-(5). At a glance, one has an impression that the profiles are not much different from those for N_2 in Fig. 1. However, the downstream half of the shock layer is much thicker. It extends over 70-80 mean free paths for $M = 1.2$. Here, the downstream half means roughly the part of the profile for $X_1 \gtrsim 0$. In Figure 3, we show the same profiles at $M = 2.0$ [Fig. 3(a)], 3.0 [Fig. 3(b)], and 5.0 [Fig. 3(c)] for CO_2-(20). The downstream half of the shock layer at $M = 2.0$ in this case is much thicker than that for CO_2-(5) [Fig. 2(b)] and reaches 50-60 mean free paths. From this fact, one can easily guess that the shock thickness at $M = 1.2$ for CO_2-(20) is very large. Therefore, a very wide computational domain is required, so that an accurate computation becomes difficult. On the other hand, each profile in Fig. 3 exhibits a double-layer structure, a steep change in the upstream half followed by a mild change in the downstream half. This separation is clearer for larger M. Therefore, we investigate the effect of increasing μ_b/μ for a fixed large M, i.e., $M = 5.0$.

Figure 4 shows the profiles of $\hat{\rho}$, $\hat{u}$, and $\hat{T}$ for CO_2-(30) [Fig. 4(a)], CO_2-(50) [Fig. 4(b)], and CO_2-(100) [Fig. 4(c)] at $M = 5.0$. As μ_b/μ increases, the double-layer structure becomes more eminent, and the downstream half becomes milder and wider. For CO_2-(100), $\hat{\rho}$ increases from nearly zero to 1/2 over one mean free path, whereas it increases from nearly 1/2 to 1 very slowly over more than 50 mean free paths. For $\hat{u}$ and $\hat{T}$, the profiles extend more toward upstream, but about 80 percent of the downstream values ($\hat{u} \simeq 0.2$, $\hat{T} \simeq 0.8$) are reached within a thin transition layer. Then the downstream values ($\hat{u} = 0$, $\hat{T} = 1$) are recovered slowly. In Fig. 5, we show the profiles of the $\hat{T}$, $\hat{T}_{\rm tr}$, and $\hat{T}_{\rm int}$ at $M = 5.0$ for CO_2-(100). Here, $\hat{T}_{\rm tr}$ and $\hat{T}_{\rm int}$ are defined by the last equation of Eq. (10) with $T = T_{\rm tr}$ and $T = T_{\rm int}$, respectively. The internal temperature $T_{\rm int}$ does not increase in the thin layer with a sharp change and is raised slowly over the thick layer. On the other hand, the translational temperature $T_{\rm tr}$ increases sharply in the thin layer and reaches

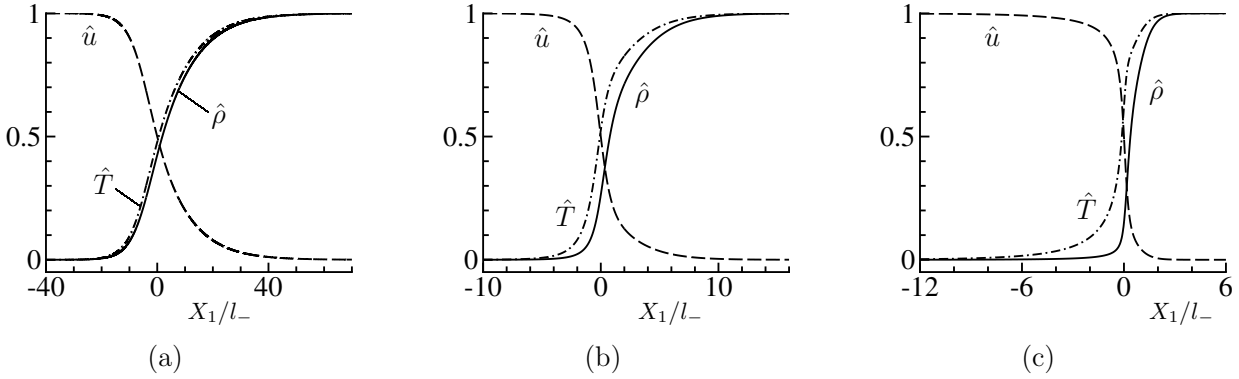

FIGURE 2. Profiles of the normalized density $\hat{\rho}$, flow velocity $\hat{u}$, and temperature $\hat{T}$ for CO_2-(5). (a) $M = 1.2$, (b) $M = 2.0$, and (c) $M = 5.0$.

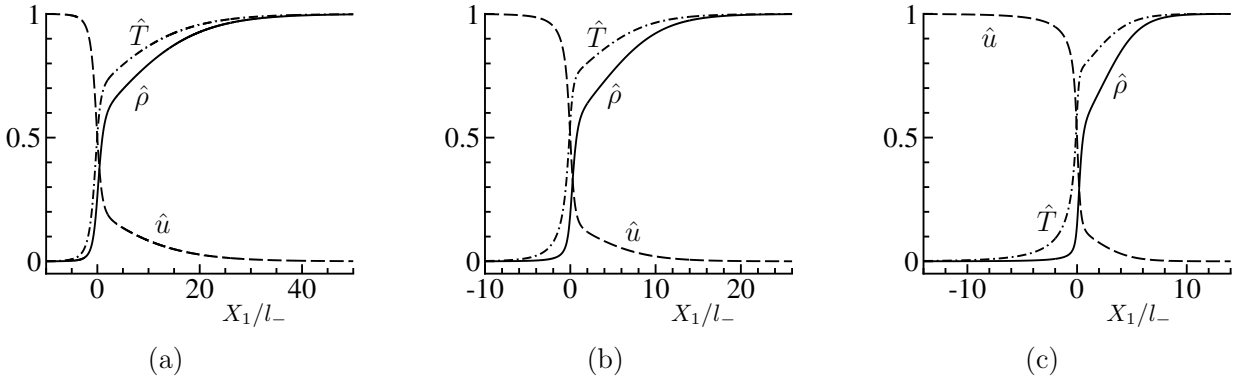

FIGURE 3. Profiles of the normalized density $\hat{\rho}$, flow velocity $\hat{u}$, and temperature $\hat{T}$ for CO_2-(20). (a) $M = 2.0$, (b) $M = 3.0$, and (c) $M = 5.0$.

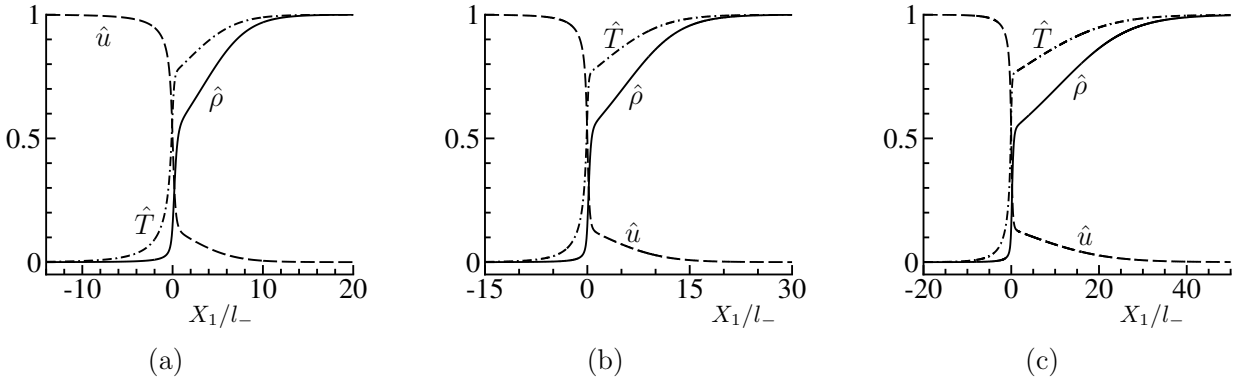

FIGURE 4. Profiles of the normalized density $\hat{\rho}$, flow velocity $\hat{u}$, and temperature $\hat{T}$ for $M = 5.0$. (a) CO_2-(30), (b) CO_2-(50), and (c) CO_2-(100).

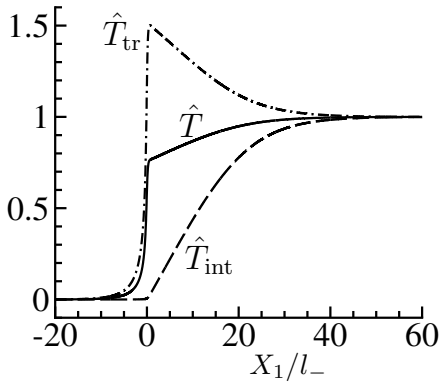

FIGURE 5. Profiles of the $\hat{T}$, $\hat{T}_{\rm tr}$, and $\hat{T}_{\rm int}$ at $M = 5.0$ for CO_2-(100).

a value that is much higher than the downstream temperature, exhibiting an overshoot.

The profiles in Fig. 4(c) have the same behavior as those obtained recently for the same Mach number on the basis of nonlinear extended thermodynamics in [9] (see Fig. 4 in [9]). The density curve shows a slight upward concavity just after the sharp transition. This feature is also observed in the result in [9].

Estimate of shock thickness for CO_2 gas and other discussions

As is seen from Fig. 4, as μ_b/μ increases, the shock thickness increases, but the thin layer with a sharp change remains the same. That is, the multi-scale nature becomes more eminent. This causes a computational difficulty because we need a wide computational domain, but at the same time, a fine grid is required to capture the sharp change. In particular, in the present preliminary study, we use a uniform grid in X_1. This is the reason why we do not carry out the computation for μ_b/μ larger than 100. This difficulty can be removed by a suitably adjusted nonuniform space grid. On the other hand, it would be interesting to estimate the shock thickness for the pseudo-CO_2 gas with μ_b/μ close to the real CO_2, say $\mu_b/\mu = 1000$.

Figure 6(a) shows the profiles of $\hat{\rho}$ at $M = 5.0$ for pseudo-CO_2 gas with $\mu_b/\mu = 5$, 10, 20, 30, 40, 50, and 100. It is seen that the upstream part with a sharp change does not depend on μ_b/μ. Let us denote by $x_{0.99}$ the value of X_1/l_- at which $\hat{\rho} = 0.99$. Since $\hat{\rho} = 1/2$ at $X_1 = 0$, $x_{0.99}$ indicates the distance (in the scale of l_-) over which $\hat{\rho}$ changes from 1/2 to 0.99. We regard this $x_{0.99}$ as the measure of the thickness of the shock profile. Figure 6(b) shows $x_{0.99}$ versus μ_b/μ for $M = 5$. The symbol indicates the value of $x_{0.99}$ at $\mu_b/\mu = 5$, 10, ..., 100, and the solid line indicates a straight line $x_{0.99} = 0.398(\mu_b/\mu) + 0.558$. As one can see, the relation between $x_{0.99}$ and μ_b/μ is almost exactly linear. If we assume that this linear relation holds for larger μ_b/μ, then $x_{0.99}$ at $\mu_b/\mu = 1000$ can become 400. That is, the thickness of the shock for CO_2 gas at $M = 5.0$ can be 400 mean free paths. On the other hand, for $\mu_b/\mu = 5$, $x_{0.99}$ at $M = 1.2$ is 17 times of $x_{0.99}$ at $M = 5.0$. If similar relation is assumed to hold for $\mu_b/\mu = 1000$, the shock thickness of CO_2 could be 6000 to 7000 mean free paths at $M = 1.2$.

The results that we have shown for pseudo-CO_2 are for $\delta = 3$, i.e., $\gamma = 4/3$. Now, we check the effect of the choice of δ. We denote by CO_2-(100′) the pseudo-CO_2 with $\mu_b/\mu = 100$ and $\delta = 4$ and by CO_2-(100″) the pseudo-CO_2 with $\mu_b/\mu = 100$ and $\delta = 2$. We compare the profiles of CO_2-(100) with those of CO_2-(100′) in Fig. 7(a) and with those of CO_2-(100″) in Fig. 7(b). In the figures, the profiles of $\hat{\rho}$, $\hat{u}$, and $\hat{T}$ are all indicated by the solid line for CO_2-(100) and by the dashed line for CO_2-(100′) [Fig. 7(a)] and for CO_2-(100″) [Fig. 7(b)]. The difference arises only in the downstream part with slow variation. In this part, there are visible differences. However, the qualitative features of the profiles remain essentially the same.

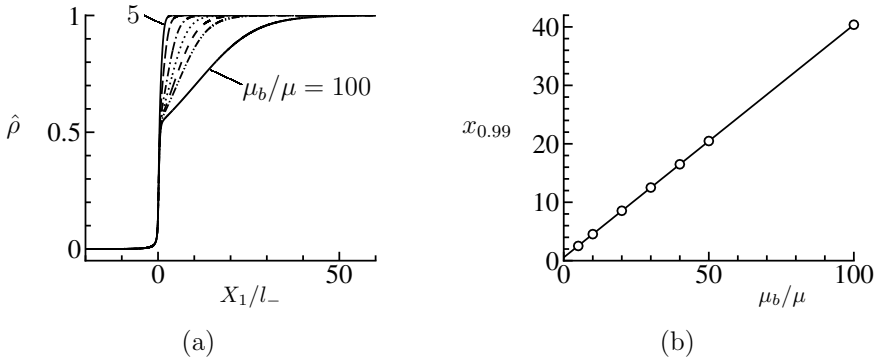

FIGURE 6. (a) Profiles of the normalized density $\hat{\rho}$ at $M = 5.0$ for pseudo-CO_2 gas with $\mu_b/\mu = 5$, 10, 20, 30, 40, 50, and 100. (b) Shock thickness $x_{0.99}$ versus μ_b/μ.

CONCLUDING REMARKS

In the present study, we investigated the structure of a plane shock wave in a polyatomic gas numerically on the basis of kinetic theory. In particular, we tried to reproduce the double-layer structure, consisting of a thin upstream layer and a thick downstream layer, peculiar to the CO_2 gas. We employed a simple model Boltzmann equation, i.e., the ES model for a polyatomic gas. Since we can practically eliminate the energy variable $\mathcal{E}$ for the internal degrees of freedom, the polyatomic effect enters the resulting equations for the marginals g, h, and i only through the parameters Pr and μ_b/μ. In addition, the model collision term has a single relaxation time. Furthermore, in this preliminary study, we only considered the pseudo-CO_2 gases with μ_b/μ much smaller than the real CO_2 gas. In spite of these simplifications, we were able to obtain the double-layer structure of the shock profile. A computation with a realistic value of μ_b/μ will be the subject of our subsequent study.

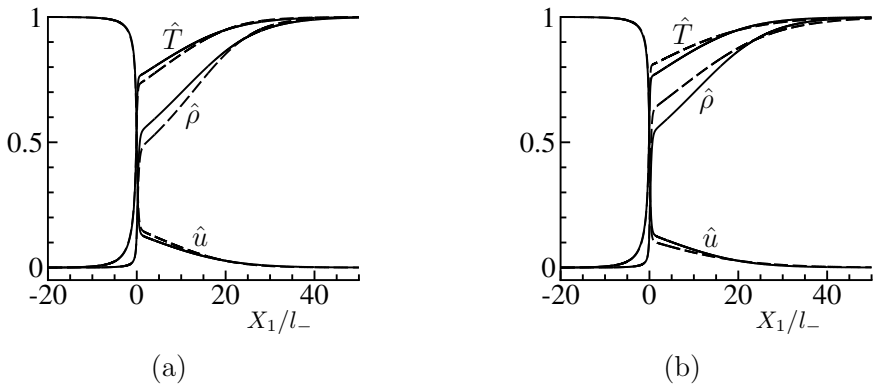

FIGURE 7. Comparision of the profiles at $M = 5.0$ for pseudo-CO_2 gas with $\mu_b/\mu = 100$. (a) CO_2-(100) and CO_2-(100′), (b) CO_2-(100) and CO_2-(100″).

ACKNOWLEDGMENTS

One of the authors (K.A.) wishes to thank AOARD for the financial support for his participation in the RGD30 Symposium. He is also grateful to National Center for Theoretical Sciences, National Taiwan University and Department of Mathematics, National Cheng Kung University for their support and hospitality.

REFERENCES

[1] M. N. Kogan, *Rarefied Gas Dynamics* (Plenum, New York, 1969).
[2] J. H. Ferziger and H. G. Kaper, *Mathematical Theory of Transport Processes in Gases* (North Holland, Amsterdam, 1972).
[3] C. Cercignani, *The Boltzmann Equation and Its Applications* (Springer, Berlin, 1988).
[4] G. A. Bird, *Molecular Gas Dynamics and the Direct Simulation of Gas Flows* (Oxford University Press, Oxford, 1994).
[5] C. Cercignani, *Rarefied Gas Dynamics: From Basic Concepts to Actual Calculations* (Cambridge Univ. Press, Cambridge, 2000).
[6] Y. Sone, *Molecular Gas Dynamics: Theory, Techniques, and Applications* (Birkhäuser, Boston, 2007).
[7] S. Taniguchi, T. Arima, T. Ruggeri, and M. Sugiyama, Phys. Rev. E **89**, 013025 (2014).
[8] T. Ruggeri and M. Sugiyama, *Rational Extended Thermodynamics beyond the Monatomic Gas* (Springer International Publishing Switzerland, 2015).
[9] S. Taniguchi, T. Arima, T. Ruggeri, and M. Sugiyama, Int. J. Non-Linear Mech. **79**, 66 (2016).
[10] L. H. Holway, Jr., Ph.D. thesis, Harvard University (1963); L. H. Holway, Phys. Fluids **9**, 1658 (1966).
[11] P. Andries, P. Le Tallec, J.-P. Perlat, and B. Perthame, Eur. J. Mech. B/Fluids **19**, 813 (2000).
[12] S. Brull and J. Schneider, Continuum Mech. Thermodyn. **20**, 489 (2009).
[13] C. Cercignani and M. Lampis, J. Stat. Phys. **26**, 795 (1981).
[14] C. K. Chu, Phys. Fluids **8**, 12 (1965).
[15] K. Aoki, Y. Sone, and T. Yamada, Phys. Fluids A **2**, 1867 (1990).
[16] G. Emanuel, Phys Fluids A **2**, 2252 (1990).
[17] F. J. Uribe, E. A. Mason, and J. Kestin, J. Phys. Chem. Ref. Data **19**, 1123 (1990).